Reprinted from Analysis Methods for Multi-Spacecraft Data
Götz Paschmann and Patrick W. Daly (Eds.),
ISSI Scientific Report SR-001

— 10 —

Shock and Discontinuity Normals, Mach Numbers, and Related Parameters

STEVEN J. SCHWARTZ
Queen Mary and Westfield College
London, United Kingdom

10.1 Introduction

Shocks and other boundaries provide key sites for mediating the mass, momentum, and energy exchange in space plasmas, and have thus been the subject of considerable research. The transient, non-planar nature of the Solar-Terrestrial interaction, however, complicates any interpretation of data from a single spacecraft. The importance of such complications, together with the importance of the boundary layer physics, is a prime motivation behind any multi-spacecraft mission. In this chapter we review the basic terminology and methodology for the determination of the most basic of parameters, such as the Mach number and the shock/discontinuity orientation. These parameters need to be established before any detailed investigation can proceed, and before any of the results thereof can be set into their proper context.

While we concentrate mainly on shocks, the methods described below apply to most "discontinuities" encountered in space plasmas, such as rotational or tangential discontinuities.

10.2 The Shock Problem: Rankine-Hugoniot Relations

The overall shock problem consists of a surface through which a non-zero mass flux flows and which effects an irreversible (i.e., entropy-increasing) transition via dissipation of some sort. At the macroscopic level, the shock must conserve total mass, momentum, and energy fluxes, together with an obeyance of Maxwell's equations. Adopting a particular macroscopic framework, such as time-stationary ideal MHD, the governing equations can be written in conservation form to reveal expressions for these fluxes in the planar (1-D) case. For example, starting from the mass continuity equation

$$\frac{\partial \rho}{\partial t} + \nabla \cdot (\rho \boldsymbol{V}) = 0 \tag{10.1}$$

only the $\hat{\boldsymbol{n}}\, d/dx_n$ operator is non-zero. In a frame in which the shock is at rest, this implies conservation of the normal mass flux and is given by

$$\rho_u (\boldsymbol{V}_u \cdot \hat{\boldsymbol{n}}) = \rho_d (\boldsymbol{V}_d \cdot \hat{\boldsymbol{n}}) \tag{10.2}$$

where $\hat{\boldsymbol{n}}$ is the shock normal and subscripts u and d denote quantities measured up- and downstream of the shock. Similar expressions can be derived for the three components of momentum carried through the shock, the energy flux, the normal magnetic field, and the two components of the tangential electric field. To these are added the frozen in field relations for the two tangential electric field components. The resulting system is 10 equations in the 10 parameters ρ, $\boldsymbol{V}$, P (the plasma thermal pressure), $\boldsymbol{B}$, and $\boldsymbol{E}_{\text{tangential}}$ on either side of the shock. This set of relations between upstream and downstream parameters is known as the Rankine-Hugoniot relations (sometimes referred to as the "shock jump conditions" although they apply across any discontinuity). If the upstream state is completely specified, these relations can be solved for the downstream state. In the case of a more complicated system, e.g., two-fluid or multi-species, there are in general fewer equations than parameters, and further assumptions concerning energy partition, etc., are required to close the system. Even in MHD, the energy conservation equation requires some closure assumptions (e.g., zero heat flux) which at best mimic the consequences of the dissipation at the shock.

10.3 Shock Parameters

There are several basic plasma parameters which characterise the media on either side of a shock. These are usually based on plasma fields and moments. This section introduces the essential parameters and shock nomenclature.

10.3.1 Shock Geometry

In a plasma permeated by a magnetic field, there are several vectors which play a role in the analysis of a shock transition. These include the bulk flow velocity, $\boldsymbol{V}$, the magnetic field, $\boldsymbol{B}$, and the shock normal, $\hat{\boldsymbol{n}}$. It is customary to orient the normal vector so that it points into the unshocked medium. In a frame in which the shock is at rest, this normal points "upstream" and the term upstream is often interchanged with "unshocked". This use of upstream and downstream can cause confusion in the case of interplanetary shocks, however, since in the spacecraft rest frame a shock propagating in the anti-sunward direction (a "forward" shock) has its unshocked medium down-wind of the shock location. Nonetheless, we will follow common practice and use the terms upstream and downstream as seen in a frame in which the shock is at rest. Accordingly, subscripts u and d will be used to denote quantities measured in the upstream and downstream media respectively.

The basic shock geometry is sketched in Figure 10.1. The various angles between $\boldsymbol{V}_u$, $\boldsymbol{B}_u$, and $\hat{\boldsymbol{n}}$ are typically denoted by a subscripted θ, e.g., θ_{Bnu} is the angle between $\boldsymbol{B}_u$ and $\hat{\boldsymbol{n}}$. Usually only the acute angles for θ_{Bnu} and θ_{Vnu} are required, but the user must be careful in analysing any given situation or in writing a generalised algorithm to cope with a rotation through 180° of the magnetic field or a normal vector which points into the downstream direction. The vector forms of the transformation velocities given below avoid such problems.

The transformation of a velocity measured in an arbitrary frame, $\boldsymbol{V}^{\text{arb}}$, (e.g., the spacecraft frame of reference) to one in which the shock is at rest is accomplished by subtracting the shock velocity in the arbitrary frame of interest. Only the normal component of the

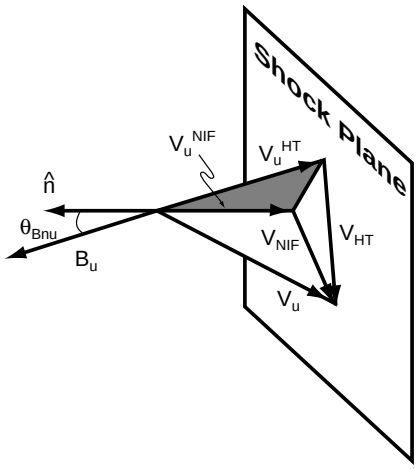

Figure 10.1: Sketch of the various vectors which enter into shock analyses. These are shown in a shock rest frame.

shock velocity, $\boldsymbol{V}_{\rm sh}^{\rm arb}$, is unique, so we shall use

$$\overset{\rm Shock}{\boldsymbol{V}^{\rm Rest}} = \boldsymbol{V}^{\rm arb} - V_{\rm sh}^{\rm arb}\hat{\boldsymbol{n}} \tag{10.3}$$

All the velocities subscripted u shown in Figure 10.1 are such shock rest frame velocities. Section 10.5 provides methods to determine $V_{\rm sh}^{\rm arb}$. There are, in fact, a multiplicity of shock rest frames, since any translation along a (planar) shock surface leaves the shock at rest. Two frames are useful:

The Normal Incidence Frame (NIF) is such that the upstream flow is directed along the shock normal. As we shall see below, it is only this component of the flow which enters into the shock Mach number.

The deHoffmann-Teller (HT) frame is such that the upstream flow is directed along the upstream magnetic field. This frame has the advantage that the $\boldsymbol{V}_u \times \boldsymbol{B}_u$ electric field vanishes. Additionally, due to the constancy of the tangential electric field across any plane layer, the flow and field are also aligned in the downstream region.

The transformation into the NIF frame from another shock rest frame is achieved via a frame velocity

$$\boldsymbol{V}_{NIF} = \hat{\boldsymbol{n}} \times \left(\boldsymbol{V}_u \times \hat{\boldsymbol{n}}\right) \tag{10.4}$$

so that in the NIF frame the upstream bulk velocity is

$$\boldsymbol{V}_u^{NIF} = \boldsymbol{V}_u - \boldsymbol{V}_{NIF} \tag{10.5}$$

It is straightforward to verify that $\boldsymbol{V}_u^{NIF}$ is parallel to $\hat{\boldsymbol{n}}$ and that the transformation velocity $\boldsymbol{V}_{NIF}$ lies in the shock plane. These vectors are shown in Figure 10.1.

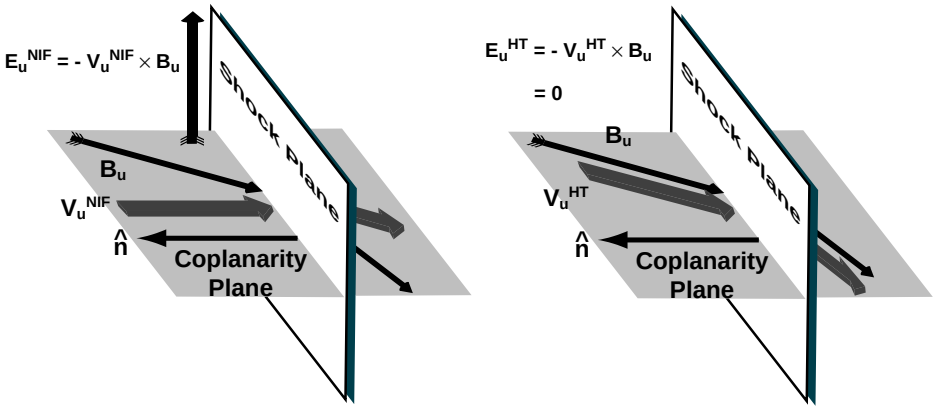

Figure 10.2: Sketch showing the various field, flow, and normal vectors in the Normal Incidence Frame (NIF) (left) and deHoffmann-Teller (HT) frame (right).

The transformation into the HT frame from another shock rest frame is achieved via a frame velocity

$$\boldsymbol{V}_{HT} = \frac{\hat{\boldsymbol{n}} \times (\boldsymbol{V}_u \times \boldsymbol{B}_u)}{\boldsymbol{B}_u \cdot \hat{\boldsymbol{n}}} \tag{10.6}$$

so that in the HT frame the upstream bulk velocity is

$$\boldsymbol{V}_u^{HT} = \boldsymbol{V}_u - \boldsymbol{V}_{HT} \tag{10.7}$$

Note that this prescription for the velocity $\boldsymbol{V}_{HT}$ is restricted to transformations only from another shock rest frame, whereas $\boldsymbol{V}_{HT}$ in Chapter 9 provides the transformation from an arbitrary (e.g., spacecraft) frame. It is straightforward to verify that $\boldsymbol{V}_u^{HT}$ is parallel to $\boldsymbol{B}_u$ and that the transformation velocity $\boldsymbol{V}_{HT}$ lies in the shock plane. These vectors are also shown in Figure 10.1. For highly oblique magnetic fields (i.e., $\theta_{Bnu} \approx 90°$) the transformation into the HT frame requires relativistic treatment, and cannot be achieved at all when $\theta_{Bnu} = 90°$.

The resulting geometries in these two frames are shown in Figure 10.2. Note that the flow and magnetic field vectors in the HT frame are aligned with one another in both the upstream and downstream regions. Also note that by the coplanarity theorem (see below) there is a single plane, the Coplanarity Plane shown in the figure and defined by the magnetic field and normal vectors, which contains the flow, magnetic field, and normal vectors on both sides of the shock surface. This plane is also shaded in Figure 10.1.

This discussion of various shock frames reveals that there is only one geometric parameter which enters the shock problem, namely θ_{Bnu}. Shocks with large values of θ_{Bnu} are called quasi-perpendicular, while those with values near zero are quasi-parallel. In the case of fast mode shocks, the separation between quasi-perpendicular and quasi-parallel is usually taken at $\theta_{Bnu} = 45°$, as this value divides the behaviour of reflected ions which participate in the shock dissipation.

10.3.2 Mach Numbers

The Mach number of a shock in an ordinary fluid is the ratio of the speed of the shock along the shock normal (i.e., $\left|\boldsymbol{V}_u \cdot \hat{\boldsymbol{n}}\right|$ in our notation) to the speed of sound in the medium upstream of the shock. In a magnetised plasma, there are three low frequency modes: the fast and slow magnetosonic waves and the intermediate (Alfvén) wave. The intermediate mode is incompressive and might not be expected to lead to a shock solution, although there has been some discussion about possible intermediate shocks in the theoretical literature. The intermediate mode does give rise to non-compressive sharp transitions, known as rotational discontinuities, in which the field (and flow) are rotated through some angle about the normal. Both the fast and slow magnetosonic waves give rise to shock solutions, known as fast and slow shocks.

Thus there are several Mach numbers of interest. The plasma counterparts to the sonic Mach number in fluids are obviously the fast Mach number, M_f, and slow Mach number, M_s, which are the ratios of the normally incident flow speed to the fast and slow MHD wave speeds in the upstream medium. These speeds are complicated by the non-isotropic nature of the MHD modes, so that the wave speeds depend on propagation direction (i.e., θ_{Bnu}). Thus an additional Mach number, the Alfvén Mach number, M_A, is often used to characterise a shock. This Mach number is calculated without regard to propagation direction, i.e.,

$$M_A = \frac{\left|\boldsymbol{V}_u \cdot \hat{\boldsymbol{n}}\right|}{|\boldsymbol{B}_u| / \sqrt{\mu_o \rho_u}} \tag{10.8}$$

The intermediate Mach number, $M_I \equiv M_A \sec\theta_{Bnu}$, is useful as it represents an upper limit to the slow Mach number. There is no upper limit to the fast Mach number, although in this case there is a "critical" Mach number, M_c, above which simple resistivity cannot provide the total shock dissipation. M_c is a function of the various shock parameters, but is at most 2.7 and usually much closer to unity. Thus many fast mode shocks in space are supercritical.

10.3.3 Important Ratios

In addition to θ_{Bnu} and the relevant shock Mach number, two more ratios are useful in parameterising shocks. One is the upstream plasma β, i.e., the ratio of plasma to magnetic pressure. The value of β controls the relative importance of the magnetic field and the level of turbulence amongst other things. At the MHD level, θ_{Bnu}, M_A, and β_u completely specify the shock problem. M_A can be replaced by any other Mach number, as they are all related via θ_{Bnu} and β_u.

The other ratio of interest is the electron to ion temperature ratio, as this controls the expected micro-instabilities.

10.4 Determination of Shock and Discontinuity Normals

There are numerous techniques aimed at determining shock normals, shock speeds, and the values of upstream and downstream plasma and field parameters which best describe the shock. Many of them rely heavily on magnetic field data, which generally

provides good time resolution together with small experimental uncertainties. The field alone, however, cannot provide the shock Mach number, heating, and other parameters, and solutions which include plasma observations are thus required. In the case of travelling interplanetary discontinuities the shocks are often weak, implying that only small changes occur in the plasma properties. This, coupled with the rather short transit time of the spacecraft in relation to the shock, increases the difficulty of the task. In the case of standing planetary bow shocks, the upstream state is the solar wind flow, which appears to the ion instruments as a collimated beam, while the downstream state is a much broader, heated population. Under such circumstances, it can be difficult to resolve both states within a single instrument to the necessary precision, and combining data from two separate instruments imposes severe cross-calibration problems which must be overcome.

In the sections which follow, we describe a variety of approaches to this problem. There is a continual trade-off amongst ease of applicability, completeness, and accuracy which must be balanced.

10.4.1 Variance Analyses

A single spacecraft passing through a 1-D structure will see variations in the magnetic field. Since $\nabla \cdot \boldsymbol{B} = 0$, the normal component of the field must remain constant. It follows that if a unique direction can be found such that the variations in magnetic field along that direction are zero (or at least minimised to a sufficient extent), then this direction corresponds to the normal direction. This method fails for pure MHD shock solutions or other cases where the variance direction is degenerate (see Chapter 8). When considering the electric field, an opposite argument holds: the tangential components of $\boldsymbol{E}$ should be continuous through such a layer, so the normal direction will correspond to that of maximum variance in $\boldsymbol{E}$. These variance techniques are described in greater detail in Chapter 8 and extended in Chapter 11 to multiple spacecraft encounters of curved surfaces, and will not be repeated here.

It is worth remembering here that, unlike all the other methods described below, the variance techniques deal with variations *within* the transition rather than the observations taken well up- and downstream of the transition. There may well be fluctuations in the upstream or downstream regions which do not lie along the shock normal (such as waves propagating along the magnetic field direction) which can give rise to difficulties if the interval selected for variance analysis is not carefully chosen and tested.

10.4.2 Coplanarity and Related Single Spacecraft Methods

The normal to a planar surface can be determined if two vectors which lie within the surface can be found. Several subsets of the Rankine-Hugoniot relations can be used to determine suitable vectors. The most widely used method relies on the Coplanarity Theorem which insists that, for compressive shocks, the magnetic field on both sides of the shock and shock normal all lie in the same plane. A corollary to this, since the only possible tangential stresses arise from the magnetic tension, is that the velocity jump across the shock also lies in this plane (as shown in Figure 10.2). The dominant change in velocity is usually along the shock normal, especially at moderate and higher Mach numbers.

Thus there are a variety of vectors which lie in the shock plane. These include the change in magnetic field (which also lies in the coplanarity plane), the cross-product of

the upstream and downstream magnetic fields (which is perpendicular to the coplanarity plane), and the cross-product between the upstream or downstream magnetic field or their difference with the change in bulk flow velocity. These vectors give rise to constraint equations for the shock normal:

$$(\Delta \boldsymbol{B}) \cdot \hat{\boldsymbol{n}} = 0 \tag{10.9}$$

$$(\boldsymbol{B}_d \times \boldsymbol{B}_u) \cdot \hat{\boldsymbol{n}} = 0 \tag{10.10}$$

$$\left(\boldsymbol{B}_u \times \Delta \boldsymbol{V}^{\mathrm{arb}}\right) \cdot \hat{\boldsymbol{n}} = 0 \tag{10.11}$$

$$\left(\boldsymbol{B}_d \times \Delta \boldsymbol{V}^{\mathrm{arb}}\right) \cdot \hat{\boldsymbol{n}} = 0 \tag{10.12}$$

$$\left(\Delta \boldsymbol{B} \times \Delta \boldsymbol{V}^{\mathrm{arb}}\right) \cdot \hat{\boldsymbol{n}} = 0 \tag{10.13}$$

We have introduced the Δ notation to indicate the jump (downstream minus upstream) in any quantity, e.g., $\Delta \boldsymbol{B} \equiv \boldsymbol{B}_d - \boldsymbol{B}_u$. In equations 10.11, 10.12 and 10.13 we have used the superscript arb (see equation 10.3) on the velocity jump to indicate that this jump can be measured in any frame (e.g., in the spacecraft frame) and not just in a shock rest frame. In principle, any pair of vectors which are dotted with $\hat{\boldsymbol{n}}$ in the above constraints can be used to find the shock normal. (A third constraint to uniquely determine $\hat{\boldsymbol{n}}$ is to make it a unit vector. The sign of $\hat{\boldsymbol{n}}$ is arbitrary and can be adjusted if required to make $\hat{\boldsymbol{n}}$ point upstream.) For example, the magnetic coplanarity normal uses the vectors in equations 10.9 and 10.10 to give

$$\hat{\boldsymbol{n}}_{MC} = \pm \frac{(\boldsymbol{B}_d \times \boldsymbol{B}_u) \times (\Delta \boldsymbol{B})}{|(\boldsymbol{B}_d \times \boldsymbol{B}_u) \times (\Delta \boldsymbol{B})|} \tag{10.14}$$

Magnetic coplanarity is easy to apply, but fails for $\theta_{Bnu} = 0°$ or $90°$. Three mixed mode normals requiring both plasma and field data are also commonly used:

$$\hat{\boldsymbol{n}}_{MX1} = \pm \frac{\left(\boldsymbol{B}_u \times \Delta \boldsymbol{V}^{\mathrm{arb}}\right) \times \Delta \boldsymbol{B}}{\left|\left(\boldsymbol{B}_u \times \Delta \boldsymbol{V}^{\mathrm{arb}}\right) \times \Delta \boldsymbol{B}\right|} \tag{10.15}$$

$$\hat{\boldsymbol{n}}_{MX2} = \pm \frac{\left(\boldsymbol{B}_d \times \Delta \boldsymbol{V}^{\mathrm{arb}}\right) \times \Delta \boldsymbol{B}}{\left|\left(\boldsymbol{B}_d \times \Delta \boldsymbol{V}^{\mathrm{arb}}\right) \times \Delta \boldsymbol{B}\right|} \tag{10.16}$$

$$\hat{\boldsymbol{n}}_{MX3} = \pm \frac{\left(\Delta \boldsymbol{B} \times \Delta \boldsymbol{V}^{\mathrm{arb}}\right) \times \Delta \boldsymbol{B}}{\left|\left(\Delta \boldsymbol{B} \times \Delta \boldsymbol{V}^{\mathrm{arb}}\right) \times \Delta \boldsymbol{B}\right|} \tag{10.17}$$

There is also an approximate normal, the velocity coplanarity normal, given by

$$\hat{\boldsymbol{n}}_{VC} = \pm \frac{\boldsymbol{V}_d^{\mathrm{arb}} - \boldsymbol{V}_u^{\mathrm{arb}}}{\left|\boldsymbol{V}_d^{\mathrm{arb}} - \boldsymbol{V}_u^{\mathrm{arb}}\right|} \tag{10.18}$$

which is an approximation, valid at high Mach numbers and for θ_{Bnu} near $0°$ or $90°$ for which magnetic stresses are unimportant, to an exact relationship based on the Rankine-Hugoniot relations.

Applying the Algorithms

All of these single spacecraft normals can be evaluated using the same overall procedures:

1. Select data intervals in both the upstream and downstream regions and find the "average" values of the required quantities.
2. Compute the normal using the formula. Adjust the sign of $\hat{\boldsymbol{n}}$ to point upstream if desired.
3. [Optional but recommended] Compare normals computed from different methods, using different averaging intervals, etc.

An alternative approach, which has been applied to both minimum variance analysis and computations of θ_{Bnu}, is to compute normals, θ_{Bnu}'s, or whatever quantity of interest from pairs of individual upstream and downstream data points and then to average the result over an ensemble of such pairs. The data points for any given pair can be chosen at random from the relevant upstream or downstream set, with subsequent replacement prior to the next choice. This approach has the advantage of providing, via the ensemble statistical deviation, an error estimate of the result.

Caveats

There are several pitfalls here, including:

1. All single spacecraft methods rely on time stationarity by assuming that upstream and downstream quantities measured at different times correspond to the same shock conditions.
2. Selecting different intervals for "average" values can lead to different results. Care should be taken to ensure that the shock layer itself is entirely excluded from these intervals.
3. Many methods fail when close to the singular cases $\theta_{Bnu} = 0°$ or 90°.
4. All methods assume planar, 1-D shock geometry.

10.4.3 Multi-Spacecraft Timings

If the same boundary passes several spacecraft, the relative positions and timings can be used to construct the boundary normal and speed, since

$$(\boldsymbol{V}_{\rm sh}^{\rm arb} t_{\alpha\beta}) \cdot \hat{\boldsymbol{n}} = \boldsymbol{r}_{\alpha\beta} \cdot \hat{\boldsymbol{n}} \tag{10.19}$$

where $\boldsymbol{r}_{\alpha\beta}$ is the separation vector between any spacecraft pair and $t_{\alpha\beta}$ the time difference between this pair for a particular boundary. Thus given 4 spacecraft, the normal vector and normal propagation velocity $V_{\rm sh}^{\rm arb} \equiv \boldsymbol{V}_{\rm sh}^{\rm arb} \cdot \hat{\boldsymbol{n}}$ are found from the solution of the following system:

$$\begin{pmatrix} \boldsymbol{r}_{12} \\ \boldsymbol{r}_{13} \\ \boldsymbol{r}_{14} \end{pmatrix} \cdot \frac{1}{V_{\rm sh}^{\rm arb}} \begin{pmatrix} n_x \\ n_y \\ n_z \end{pmatrix} = \begin{pmatrix} t_{12} \\ t_{13} \\ t_{14} \end{pmatrix} \tag{10.20}$$

This problem is also addressed elsewhere within this book, e.g., in Chapters 12 (Sections 12.1.2 and 12.2), 14 (Section 14.5.2) and the entire Chapter 11.

Algorithm

Solve the system 10.20 for $\hat{\boldsymbol{n}}/V_{\rm sh}^{\rm arb}$ (to within the $\pm$ sign arbitrariness for $\hat{\boldsymbol{n}}$) by any standard linear algebra technique, e.g., by inverting the matrix on the left containing the separation vectors.

Caveats

1. If the separation vectors are large, the assumption of planarity may breakdown.
2. Spacecraft positions are often given in non-stationary systems, such as GSE. Since the origin of such systems moves (especially $y_{\rm GSE}$) with time, spacecraft positions should be placed onto a common coordinate system.
3. The method fails if the spacecraft are nearly coplanar. This is discussed further in Chapters 12 and 14, and illustrated numerically in Chapter 15.

10.4.4 Combined Approaches

Provided some multi-spacecraft timings are available, it is possible to add to the system 10.20 any (or all) of the constraints given in Section 10.4.2. For example, consider the system

$$\mathsf{A}\cdot(\hat{\boldsymbol{n}}/V_{\rm sh}^{\rm arb}) \equiv \begin{pmatrix} \boldsymbol{r}_{12} \\ \boldsymbol{r}_{13} \\ \boldsymbol{r}_{14} \\ \Delta\boldsymbol{B} \\ \Delta\boldsymbol{B}\times\Delta\boldsymbol{V}^{\rm arb} \end{pmatrix} \cdot \frac{1}{V_{\rm sh}^{\rm arb}} \begin{pmatrix} n_x \\ n_y \\ n_z \end{pmatrix} = \begin{pmatrix} t_{12} \\ t_{13} \\ t_{14} \\ 0 \\ 0 \end{pmatrix} \tag{10.21}$$

which makes use of equations 10.9 and 10.13.

Algorithm

The system 10.21 of equations is over-determined. The least squares solution which minimises the residuals on the right-hand side can be obtained by multiplying on the left throughout by the transpose of the matrix of coefficients A and solving the resulting 3×3 square system for $\hat{\boldsymbol{n}}/V_{\rm sh}^{\rm arb}$ (to within the $\pm$ sign arbitrariness for $\hat{\boldsymbol{n}}$). This approach has the advantage in that it can fold in more information and can be used when not all the quantities are known (e.g., when one spacecraft is missing).

Caveats

1. The least squares solution as described above takes no account of the relative errors or confidence in the various coefficients contained in A. More general inversion techniques (e.g., singular value decomposition) provide some error analyses, and can weight the different constraint equations differently to reduce the residual errors. There are probably methods which can include the possibility of different error estimates for individual components of A, but they have not yet been applied to these kinds of problems.

2. Some caution should be taken to ensure that the same information is not included many times in extending the system of equations to be solved.

3. The nature of the information contributed by multi-spacecraft timing depends upon the spatial geometry of the polyhedron defined by the spacecraft (see Chapter 12). The effect of this upon the combined approach merits further study.

10.4.5 Shock Jump Conditions

The previous methods use a small subset of the Rankine-Hugoniot relations and/or multi-spacecraft timings to determine the shock normal. A potentially more reliable approach is to take more of the Rankine-Hugoniot relations into account in order to establish a full set of upstream and downstream quantities (including the shock normal direction) which best satisfy these physical laws. Since the thermal properties of the shock processes often involve kinetic and anisotropic processes, multi-species, etc., it is probably best to avoid as much as possible those relations that involve the plasma pressure, namely the $\hat{\boldsymbol{n}}$-momentum equation and the energy flux equation. The pressure jump can then be used to verify that the resulting solution does in fact represent a compressive, entropy-producing shock.

Lepping and Argentiero first put such a scheme together in 1971, although their method still relied on magnetic coplanarity to establish the shock normal direction. Viñas and Scudder (VS) overcame this difficulty in 1986. Although the method is too lengthy to be repeated here, we describe the overall philosophy and approach for reference.

VS begin with a set of pairs of measurements of the plasma parameters (ρ, $\boldsymbol{V}$, $\boldsymbol{B}$) on either side of the shock in an arbitrary frame of reference. Equation 10.3 is used to write the Rankine-Hugoniot relations for mass flux, normal magnetic field, tangential stress, and tangential electric field in an arbitrary frame of reference. The shock speed, $V_{\mathrm{sh}}^{\mathrm{arb}}$, enters linearly in the mass flux balance equation and can be eliminated. Treating the plasma parameters as known (from the observations) leads to a system of 7 equations in which the only unknowns are the two angles which define the shock normal direction. This nonlinear system is solved via a least squares method for these two angles. Once the normal is found, the shock speed can be found from the mass flux equation as the average of the shock speed inferred from individual pairs of up- and downstream measurements. This solution minimises in a least squares sense the residuals from the shock speed as inferred by the individual pairs.

Next, in a manner identical to that used to find $V_{\mathrm{sh}}^{\mathrm{arb}}$, the conservation constants for the mass flux, normal magnetic field, tangential stress, and tangential electric field can be evaluated as the averages of their values deduced from individual pairs of observations.

Next, using these conservation constants, VS set up a least squares problem to establish the self-consistent asymptotic states via two vector equations for $\boldsymbol{V}$ and $\boldsymbol{B}$ parameterised in terms of the mass density. The value of ρ which minimises the residuals in these equations then determines the asymptotic values of the various parameters.

Finally, the normal momentum equation can be used to test that the inferred jump in thermal pressure, as demanded by the asymptotic values of the other parameters, has the correct sign.

Algorithm

See the VS reference for a more detailed account of the algorithm.

Caveats

1. These methods also rely on the selection of suitable upstream and downstream intervals of data, and on pairing an upstream observation with a downstream one.
2. The usual caveats concerning stationarity and planarity apply.
3. The potential advantage of bringing more plasma parameters to bear on the problem has the potential disadvantage that it places more emphasis on quantities, such as the plasma mass density, which may not be particularly accurate.

10.4.6 Model Boundary Equations

In the case of the Earth's bow shock and magnetopause and, to perhaps a lesser extent, those at other planets, the large number of spacecraft encounters enables us to define the shape of the boundary surface on a statistical basis. Such statistical data sets can be fit by simple geometrical forms, from which the normal direction can be computed analytically. This method is straightforward, and the algorithm is described below. In many instances, such normals are likely to be as accurate as any of those computed above.

To begin, choose an appropriate model. Most are cylindrically symmetric conic sections which can thus be represented in the form

$$\frac{L}{r^{abd}} = 1 + \epsilon \cos\theta^{abd} \tag{10.22}$$

in which L is the semilatus rectum and ϵ the eccentricity of the conic. The variables r^{abd} and θ^{abd} are polar coordinates in the natural system for the conic. This natural system is aberrated by an angle α from GSE by, e.g., the Earth's orbital motion (30 km/s so that $\tan\alpha = 30\,\mathrm{km/s}/V_{\text{solar wind}}$) and then perhaps displaced from the Earth's centre. Thus the relevant variable transformation is

$$\begin{pmatrix} x^{abd} \\ y^{abd} \\ z^{abd} \end{pmatrix} = \begin{pmatrix} \cos\alpha & -\sin\alpha & 0 \\ \sin\alpha & \cos\alpha & 0 \\ 0 & 0 & 1 \end{pmatrix} \cdot \begin{pmatrix} x \\ y \\ z \end{pmatrix} - \begin{pmatrix} x_o \\ y_o \\ z_o \end{pmatrix} \tag{10.23}$$

where $\boldsymbol{r}_o$ is the displacement of the focus of the conic in the aberrated frame and $\boldsymbol{r}$ is a position vector in the relevant observational frame (e.g., GSE). This configuration is sketched in Figure 10.3.

Different models give different values for ϵ, L, and $\boldsymbol{r}_o$. Some popular models are tabulated in Table 10.1. These models are also shown in Figure 10.4 for comparison. In any application, it may also be necessary to scale the distances (L and $\boldsymbol{r}_o$) which appear in the models. For example, the bow shock and magnetopause respond to changes in the dynamic pressure in the solar wind. The expected spatial variation is proportional to the dynamic pressure to the power $-1/6$, due to the balance with the magnetic pressure which the Earth's dipole field is able to exert. An alternative approach is to scale the distances to make the model pass through an observed location.

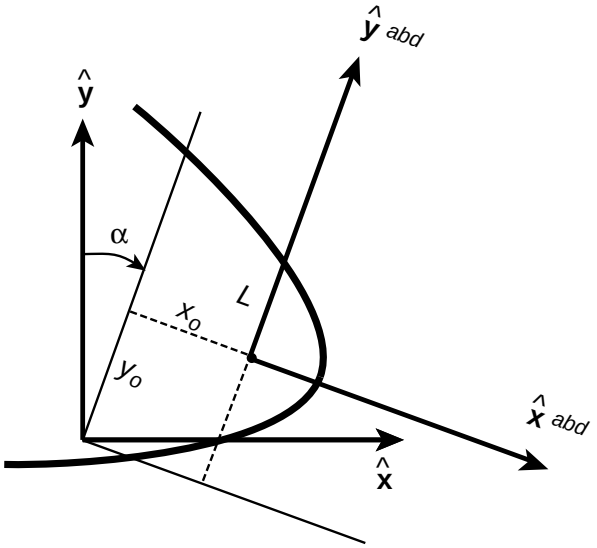

Figure 10.3: Observational (e.g., GSE) coordinate system (x, y) and aberrated-displaced system (x^{abd}, y^{abd}) for model boundaries. For simplicity, only a two-dimensional system is shown. Note that the direction of α is defined such that positive values correspond to the aberration due to the Earth's orbital motion, which is in the $-\hat{\boldsymbol{y}}$ direction.

Algorithm

1. Choose an appropriate model. For measurements under unusual circumstances or at high latitudes, consider the parameterised 3-D models by *Peredo et al.* and *Roelof and Sibeck* for the bow shock and magnetopause respectively.

2. Calculate the aberration angle as given in the model or via a measurement of the solar wind speed. If solar wind data is not present, a typical value of 450 km/s, corresponding to $\alpha = 3.8°$, is usually adequate.

3. Scale L and $\boldsymbol{r}_o$ as necessary. One way is by the $-1/6$ power of the solar wind ram pressure, normalised to the model mean as given in Table 10.1. This process is not particularly accurate and produces far less variation in, say, the bow shock position than is actually observed. Thus well upstream of the bow shock the absolute position of the bow shock can be uncertain by several R_E. Alternatively scale these parameters so that the model passes through a given position vector $\boldsymbol{r}_{\text{crossing}}$. This process can be reduced to the substitutions $L \rightarrow \sigma L$, $\boldsymbol{r}_o \rightarrow \sigma \boldsymbol{r}_o$, and $\boldsymbol{r} \rightarrow \boldsymbol{r}_{\text{crossing}}$ in equations 10.22 and 10.23 and solving the resulting quadratic equation for σ. In the case of hyperbolic ($\epsilon > 1$) models, the larger of the two roots corresponds to the correct branch of the hyperbola.

4. Calculate the gradient, ∇S, to the surface given by the model. This surface may be

Table 10.1: Parameter values for various model surfaces

Source Units	ϵ	L R_E	x_o R_E	y_o R_E	α °	ρV_{sw}^2 nPa
Terrestrial Bow Shock Models						
Peredo et al., $z = 0$	0.98	26.1	2.0	0.3	α_o-0.6	3.1
Slavin and Holzer mean	1.16	23.3	3.0	0.0	α_o	2.1
Fairfield Meridian 4°	1.02	22.3	3.4	0.3	4.8	?
Fairfield Meridian No 4°	1.05	20.5	4.6	0.4	5.2	?
Formisano Unnorm. $z = 0$	0.97	22.8	2.6	1.1	3.6	3.7
Farris et al.	0.81	24.8	$\equiv 0$	$\equiv 0$	3.8	1.8
Terrestrial Magnetopause Models						
Roelof and Sibeck (F_{00} only)	0.91	11.2	4.82	$\equiv 0$	α_o	2.1
Fairfield Meridian 4°	0.79	13.1	3.6	0.4	-0.3	?
Fairfield Meridian No 4°	0.80	12.8	3.9	0.6	-1.5	?
Farris et al.	0.43	14.7	$\equiv 0$	$\equiv 0$	3.8	1.8
Petrinec et al., ($B_z > 0$)	0.42	14.6	$\equiv 0$	$\equiv 0$	α_o	~ 2.5
Petrinec et al., ($B_z < 0$)	0.50	14.6	$\equiv 0$	$\equiv 0$	α_o	~ 2.5
Formisano						
Unnorm. $z = 0$	0.82	12.5	4.1	0.1	4.2	3.7
Norm. $z = 0$	0.69	13.5	0.9	-0.4	6.6	3.7

Notes: The above table shows aberration angles positive when in the nominal sense for the Earth's orbital motion, as shown in Figure 10.3. The value α_o indicates that each data point was aberrated by the amount corresponding to the prevailing solar wind speed. The average solar wind dynamic pressure, where available, is also shown. All models have $z_o \equiv 0$. Non-axially symmetric models have been reduced to polar form after setting $z = 0$ in the model equation.

written

$$S(\boldsymbol{r}^{abd}(x, y, z)) \equiv \left(r^{abd} + \epsilon x^{abd}\right)^2 - L^2 = 0 \tag{10.24}$$

This gradient, expressed in terms of the aberrated coordinates $\boldsymbol{r}^{abd}$ but rotated back into the unaberrated coordinate frame can be written

$$\left(\frac{r^{abd}}{2L}\nabla S\right) = \begin{pmatrix} \left[x^{abd}\left(1-\epsilon^2\right) + \epsilon L\right]\cos\alpha + y^{abd}\sin\alpha \\ -\left[x^{abd}\left(1-\epsilon^2\right) + \epsilon L\right]\sin\alpha + y^{abd}\cos\alpha \\ z^{abd} \end{pmatrix} \tag{10.25}$$

5. The normal $\hat{\boldsymbol{n}}$ is parallel to this gradient, i.e.,

$$\hat{\boldsymbol{n}} = \pm\frac{\nabla S}{|\nabla S|} \tag{10.26}$$

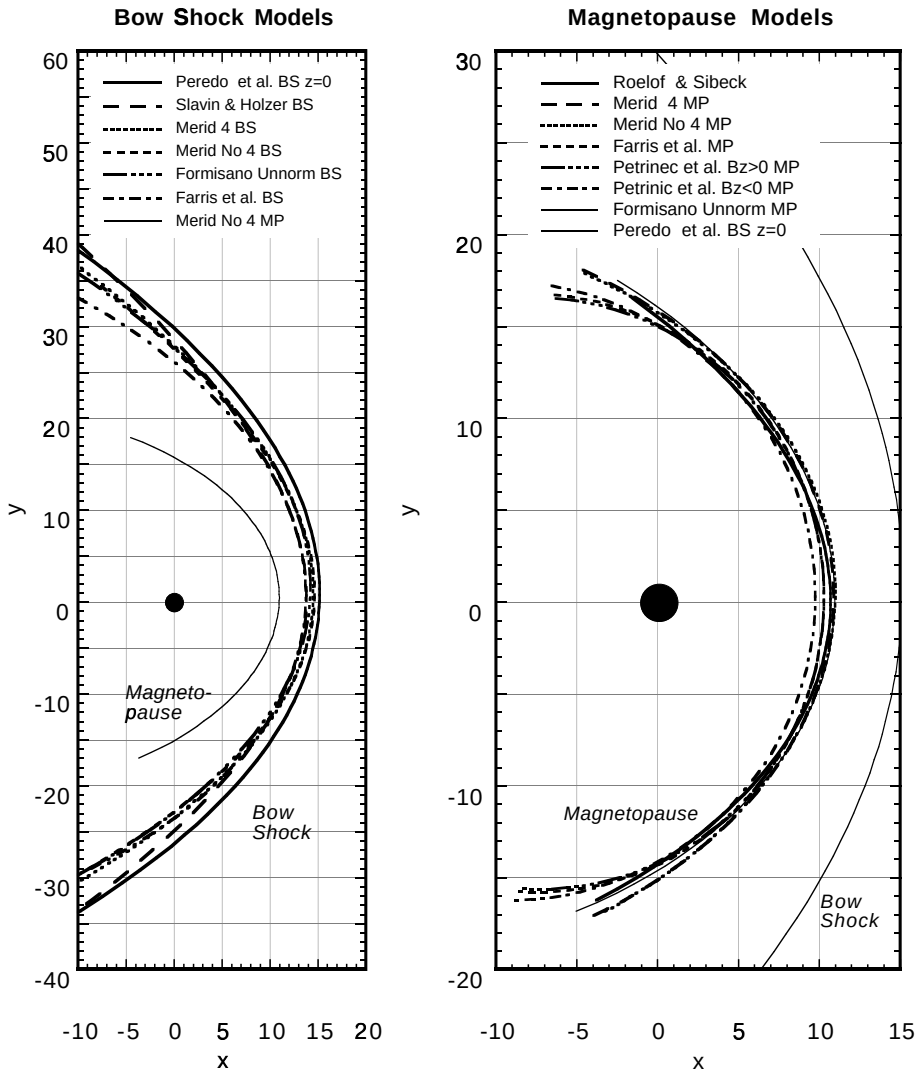

Figure 10.4: Dayside portions of model terrestrial bow shocks (left) and magnetopauses (right) based on the parameters given in Table 10.1. The models have not been scaled and have been aberrated by the amount shown in the table with $\alpha_o = 3.8°$. For the purposes of estimating shock normals, most models agree to a fair degree. The magnetopause tailward of the terminator ($x = 0$) and/or at high latitudes is more complex, and varies most with interplanetary conditions. Some models include non-axially symmetric terms. These are shown in the ecliptic plane only (see the bibliography for more details).

Caveats

1. There may be ripples or transients which distort $\hat{\boldsymbol{n}}$ from the model value.
2. Scaling the distances can be imprecise when the spacecraft is not at an actual crossing.
3. There are a multiplicity of models although, as shown in Figure 10.4, there is not a large variation in the normal direction at a given position, at least for the dayside portions and under nominal interplanetary conditions.
4. At greater tailward distances the bow shock models need to be modified to asymptote to the fast mode Mach cone (see Slavin, J. A., Holzer, R. E., Spreiter, J. R., and Stahara, S. S., Planetary Mach cones: Theory and observation, *J. Geophys. Res.*, **89**, 2708–2714, 1984).

10.4.7 Tangential Discontinuities

In the case of pure tangential discontinuities, it is possible to find the normal to the discontinuity by simply noting that both upstream and downstream magnetic field vectors are parallel to the shock plane and, unlike the case of a perpendicular shock, are not in general parallel to one another. Thus in this case the normal is given by

$$\hat{\boldsymbol{n}} = \pm \frac{\boldsymbol{B}_u \times \boldsymbol{B}_d}{\left|\boldsymbol{B}_u \times \boldsymbol{B}_d\right|} \tag{10.27}$$

Caveats

The problem here is to use sufficient plasma and field variations, particularly the pressures, to establish that the discontinuity in question is indeed a tangential discontinuity and not a rotational discontinuity or a slow shock. Since all the pressures rise across a fast shock, it is usually easier to distinguish these from the pressure balance structures required by tangential discontinuities, although weak shocks may again prove difficult.

10.4.8 Rotational Discontinuities

If sufficient field resolution is present, minimum variance analysis of the magnetic field, or maximum variance of the electric field, provides an estimate of the normal direction. The caveats given above concerning the identification of tangential discontinuities also apply here.

10.5 Determination of the Shock/Discontinuity Speed

The shock speed along the normal, $\boldsymbol{V}_u \cdot \hat{\boldsymbol{n}}$, is a vital parameter, as it determines the shock Mach number. There are a variety of methods in use to calculate this speed from observational data, or to calculate the shock speed relative to an arbitrary observational frame, $V_{\mathrm{sh}}^{\mathrm{arb}}\hat{\boldsymbol{n}}$, which are summarised here. These velocities are related by equation 10.3. Most of the following methods also require knowledge of the shock normal.

10.5.1 Mass Flux Algorithm

Writing the shock mass flux conservation equation in terms of quantities measured in an arbitrary frame yields

$$\rho_u(\boldsymbol{V}_u^{\text{arb}} - V_{\text{sh}}^{\text{arb}}\hat{\boldsymbol{n}}) \cdot \hat{\boldsymbol{n}} = \rho_d(\boldsymbol{V}_d^{\text{arb}} - V_{\text{sh}}^{\text{arb}}\hat{\boldsymbol{n}}) \cdot \hat{\boldsymbol{n}} \tag{10.28}$$

This equation can be solved for $V_{\text{sh}}^{\text{arb}}$ to give

$$V_{\text{sh}}^{\text{arb}} = \frac{\Delta(\rho \boldsymbol{V}^{\text{arb}})}{\Delta\rho} \cdot \hat{\boldsymbol{n}} \tag{10.29}$$

Caveats

The only difficulty applying equation 10.29 is its reliance on good plasma density measurements on both sides of the shock.

10.5.2 Shock Foot Thickness Algorithm

Quasi-perpendicular supercritical collisionless shocks initiate their dissipation process by reflecting a portion of the incoming ion distribution. Under these geometries, such reflected ions gyrate around the magnetic field in front of the main shock ramp and return to the shock. The extent of this foot region in front of such shocks is directly related to these reflected ion trajectories which, in turn, are simply related to the incident normal velocity (in a shock rest frame), the strength of the field, and the shock geometry. The shock foot is clearly visible as a gradual rise in the magnetic field, and can also be found in the commencement of ion-acoustic-like noise upstream of the shock ramp. Assuming the incident ions are specularly reflected at the shock, and neglecting their thermal motion, the reflected ions reach their maximum upstream excursion and turn around after a time t_{turn} which is the solution to

$$\cos(\Omega t_{\text{turn}}) = \frac{1 - 2\cos^2\theta_{Bnu}}{2\sin^2\theta_{Bnu}} \tag{10.30}$$

where Ω is the ion gyrofrequency. At this time, their distance, d_{foot}, along the normal from the shock ramp is

$$\frac{d_{\text{foot}}}{(\boldsymbol{V}_u \cdot \hat{\boldsymbol{n}})/\Omega} \equiv f(\theta_{Bnu}) = \Omega t_{\text{turn}}\left(2\cos^2\theta_{Bnu} - 1\right) + 2\sin^2\theta_{Bnu}\sin(\Omega t_{\text{turn}}) \tag{10.31}$$

Knowing the time Δt_{foot} taken for the foot to pass over a point in an arbitrary observational frame (e.g., the spacecraft frame) then provides the additional information required, resulting in

$$\boldsymbol{V}_u \cdot \hat{\boldsymbol{n}} = \frac{\boldsymbol{V}_u^{\text{arb}} \cdot \hat{\boldsymbol{n}}}{1 \mp (f(\theta_{Bnu})/\Omega\Delta t_{\text{foot}})} \tag{10.32}$$

The upper $(-)$ sign is used when the observed transition is from upstream to downstream and the lower $(+)$ when the observed sequence is downstream to upstream.

Algorithm

1. Measure the foot passage time Δt_{foot}. Determine θ_{Bnu} from the data by either finding $\hat{\boldsymbol{n}}$ and $\boldsymbol{B}_u$ or by an algorithm given below in Section 10.6.

2. Compute $f(\theta_{Bnu})$.

3. Apply equation 10.32.

Caveats

1. This is quite a good method for these shocks, but requires a good methodology for identifying the foot region.

2. The method requires that the relative shock/observer motion be steady during the passage of the foot.

10.5.3 Multi-Spacecraft Timing Algorithm

This approach for determining shock speeds is detailed above in Sections 10.4.3 and 10.4.4.

10.5.4 Smith and Burton Algorithm

Smith and Burton have derived an algorithm to determine the shock speed which does not require an explicit calculation of the shock normal. Their algorithm is derived from the Rankine-Hugoniot relation which represents continuity of the tangential electric field [$-\hat{\boldsymbol{n}} \times (\boldsymbol{V}_u \times \boldsymbol{B}_u) = -\hat{\boldsymbol{n}} \times (\boldsymbol{V}_d \times \boldsymbol{B}_d)$ in our notation]. Some manipulation and implicit use of the coplanarity theorem yields

$$\left|\boldsymbol{V}_u \cdot \hat{\boldsymbol{n}}\right| = \frac{\left|\Delta \boldsymbol{V}^{\text{arb}} \times \boldsymbol{B}_d\right|}{|\Delta \boldsymbol{B}|} \tag{10.33}$$

Caveats

1. This algorithm requires a good vector determination of $\Delta \boldsymbol{V}^{\text{arb}}$.

2. The algorithm works for all shock geometries, including parallel "switch on" shocks, but breaks down for parallel acoustic shocks, which have $\boldsymbol{B}_d = \boldsymbol{B}_u$.

10.5.5 Generalised deHoffmann-Teller Transformation

Chapter 9 shows how the transformation velocity from an arbitrary spacecraft frame to the deHoffmann-Teller frame can be found if there are good determinations of the flow velocity and field on both sides of the shock transition. The shock velocity along the normal $V_{\text{sh}}^{\text{arb}}$ is simply the normal component of the generalised HT-frame velocity, as shown in Figure 9.2 (page 225) of Chapter 9.

Algorithm

1. Use the methods in Chapter 9 to determine the velocity of the deHoffmann-Teller frame with respect to an arbitrary (e.g., spacecraft) frame.

2. Take the normal component of this velocity

10.5.6 Velocity of a Tangential Discontinuity

Since a tangential discontinuity has, by definition, zero mass flux through the discontinuity layer, in a rest frame moving with the discontinuity the flow velocities on either side have only tangential components. Thus in an arbitrary frame of reference, the component of the flow velocity normal to the discontinuity must equal the speed of the discontinuity, i.e.,

$$V_{TD}^{\text{arb}} = \boldsymbol{V}^{\text{arb}} \cdot \hat{\boldsymbol{n}} \tag{10.34}$$

This should produce the same result regardless of whether the upstream or downstream flow velocity is used.

Algorithm

1. Apply equation 10.34 using a measured flow velocity and a normal vector determined by, e.g., equation 10.27.

2. [Optional] Apply equation 10.34 for flow velocities measured both upstream and downstream of the discontinuity to provide some estimate of the error.

Caveats

1. The difference between values computed using upstream and downstream values may be due to either errors in the measured flow velocities, in the discontinuity normal determination, or both.

10.6 Determining θ_{Bnu}

10.6.1 Application of the Shock Normal

Algorithm

1. Determine $\hat{\boldsymbol{n}}$ via one of the algorithms given in Section 10.4.

2. Determine $\boldsymbol{B}_u$ in a manner consistent with that used for $\hat{\boldsymbol{n}}$. That is, if averages of upstream parameters are used to find $\hat{\boldsymbol{n}}$, use the same $\boldsymbol{B}_u$.

3. $\theta_{Bnu} = \cos^{-1}(\hat{\boldsymbol{n}} \cdot \boldsymbol{B}_u / |\boldsymbol{B}_u|)$.

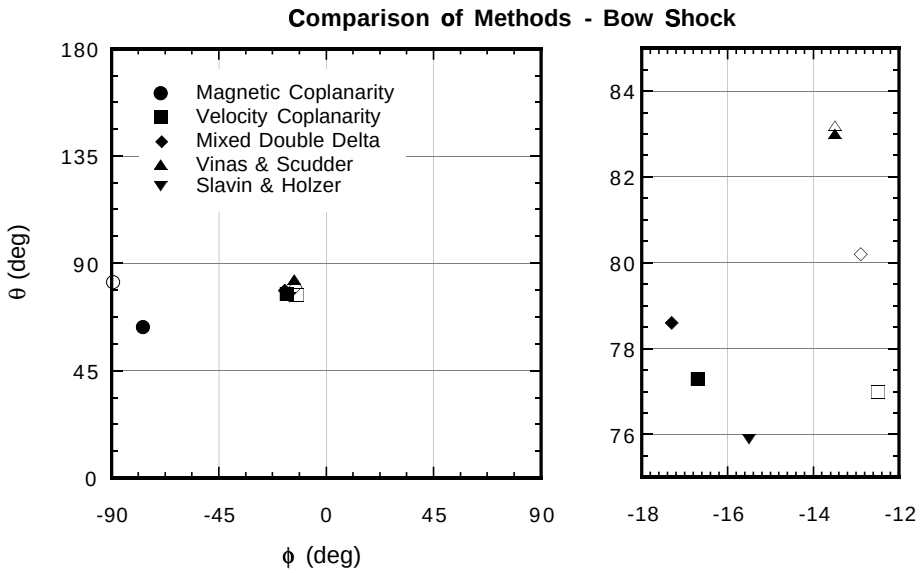

Figure 10.5: Normal directions based on several of the methods given in this chapter as applied to a particular crossing of the Earth's bow shock. The normals are given in terms of their spherical polar angles in the GSE frame: $\theta = 0°$ is along $\hat{z}$ while $\phi = 0°$ is the sunward direction. Open symbols use the same methods as their solid counterparts but use input up- and downstream parameters averaged over fewer observational data points. Note the failure of magnetic coplanarity in this case due to the near perpendicular shock geometry ($\theta_{Bnu} \sim 80°$ in this case). The right panel shows in detail the spread of the other methods and reveals a typical uncertainty of $5 - 10°$ or more.

10.6.2 Ensemble θ_{Bnu}

Algorithm

1. Apply the previous algorithm (e.g., using $\hat{\boldsymbol{n}}$) to pairs of upstream and downstream data points.

2. Ensemble average the results to provide $\langle\theta_{Bnu}\rangle$ together with its standard deviation.

10.7 Application

As an example of many of the above methods, we present here the results of normal determination for a particularly well-studied example of the Earth's bow shock. Figure 10.5 shows the results of several coplanarity-like techniques, the Rankine-Hugoniot solution of Viñas and Scudder, and a bow shock model normal. Most methods agree to within $5-10°$, although the magnetic coplanarity technique fails badly here due to the near perpendicular orientation of the upstream field in this case. Of course, the determination of θ_{Bnu} itself

varies with the different normals, and thus has a similar uncertainty. The choice of method may depend on the particular case. Ideally, different methods should be compared with one another.

Bibliography

Two AGU Monographs provide a wealth of information relating to shock physics:

Kennel, C. F., A quarter century of collisionless shock research, in *Collisionless Shocks in the Heliosphere: A Tutorial Review*, edited by R. G. Stone and B. T. Tsurutani, AGU Monograph 34, pp. 1–36, American Geophysical Union, Washington, D. C., 1985, covers in some detail the various shock modes, critical Mach numbers, and the like.

Tsurutani, B. T. and Stone, R. G., editors, *Collisionless Shocks in the Heliosphere: Reviews Of Current Research*, AGU Monograph 35, American Geophysical Union, Washington, D. C., 1985, is the companion monograph containing much useful material.

A good basic introduction to collisionless shocks and discontinuities, including the Rankine-Hugoniot relations, shock frames and geometry, and shock structure/processes can be found in:

Burgess, D., Collisionless shocks, in *Introduction to Space Physics*, edited by M. G. Kivelson and C. T. Russell, pp. 129–163, Cambridge University Press, Cambridge, U. K., 1995.

The seminal work on the subject of shock normal determination by multiple satellite techniques, and a work that applies it in detail, are:

Russell, C. T., Mellott, M. M., Smith, E. J., and King, J. H., Multiple spacecraft observations of interplanetary shocks: Four spacecraft determination of shock normals, *J. Geophys. Res.*, **88**, 4739–4748, 1983.

Russell, C. T., Gosling, J. T., Zwickl, R. D., and Smith, E. J., Multiple spacecraft observations of interplanetary shocks: ISEE three-dimensional plasma measurements, *J. Geophys. Res.*, **88**, 9941–9947, 1983.

The Rankine-Hugoniot approach to shock normal and parameter determination is detailed in:

Viñas, A. F. and Scudder, J. D., Fast and optimal solution to the "Rankine-Hugoniot problem", *J. Geophys. Res.*, **91**, 39–58, 1986.

Scudder, J. D., Mangeney, A., Lacombe, C., Harvey, C. C., Aggson, T. L., Anderson, R. R., Gosling, J. T., Paschmann, G., and Russell, C. T., The resolved layer of a collisionless, high β, supercritical quasi-perpendicular shock wave, 1. Rankine-Hugoniot geometry, currents, and stationarity, *J. Geophys. Res.*, **91**, 11 019–11 052, 1986, contains the data for the comparison shown in Figure 10.5.

A partial approach to the Rankine-Hugoniot problem was presented originally by:

Lepping, R. P. and Argentiero, P. D., Single spacecraft method of estimating shock normals, *J. Geophys. Res.*, **76**, 4349, 1971

The above approach was modified further in:

Acuña, M. H. and Lepping, R. P., Modification to shock fitting program, *J. Geophys. Res.*, **89**, 11 004, 1984.

The velocity coplanarity method is presented in:

Abraham-Shrauner, B., Determination of magnetohydrodynamic shock normals, *J. Geophys. Res.*, **77**, 736, 1972.

Abraham-Shrauner, B. and Yun, S. H., Interplanetary shocks seen by Ames probe on Pioneer 6 and 7, *J. Geophys. Res.*, **81**, 2097, 1976, applied it further

Smith, E. J. and Burton, M. E., Shock analysis: 3 useful new relations, *J. Geophys. Res.*, **93**, 2730–2734, 1988, who proposed additional relations.

The boundary models shown in Table 10.1 have been derived from the following references:

Peredo, M., Slavin, J. A., Mazur, E., and Curtis, S. A., Three-dimensional position and shape of the bow shock and their variation with Alfvénic, sonic and magnetosonic Mach numbers and interplanetary magnetic field orientation, *J. Geophys. Res.*, **100**, 7907–7916, 1995. [The parameters shown in Table 10.1 correspond to their full M_A range $< 2 - 20 >$, p-normalised and GIPM rotated.]

Slavin, J. A. and Holzer, R. E., Solar wind flow about the terrestrial planets, 1. modelling bow shock position and shape, *J. Geophys. Res.*, **86**, 11 401–11 418, 1981. [The values in Table 10.1 correct errors in the original paper. Also, there is an unrelated typographical error there: the k_3' equation should have a "+" sign in front of the middle (k_2) term. (J. A. Slavin, private communication, 1997)].

See also Slavin, J. A., Holzer, R. E., Spreiter, J. R., and Stahara, S. S., Planetary Mach cones: Theory and observation, *J. Geophys. Res.*, **89**, 2708–2714, 1984.

Fairfield, D. H., Average and unusual locations of the Earth's magnetopause and bow shock, *J. Geophys. Res.*, **76**, 6700–6716, 1971.

Formisano, V., Orientation and shape of the Earth's bow shock in three dimensions, *Planet. Space Sci.*, **27**, 1151–1161, 1979.

Farris, M. H., Petrinec, S. M., and Russell, C. T., The thickness of the magnetosheath: Constraints on the polytropic index, *Geophys. Res. Lett.*, **18**, 1821–1824, 1991.

Roelof, E. C. and Sibeck, D. C., Magnetopause shape as a bivariate function of interplanetary magnetic field b_z and solar wind dynamic pressure, *J. Geophys. Res.*, **98**, 21 421–21 450, 1993.

Roelof, E. C. and Sibeck, D. C., Correction to "magnetopause shape as a bivariate function of interplanetary magnetic field b_z and solar wind dynamic pressure", *J. Geophys. Res.*, **99**, 8787–8788, 1994.

See also Holzer, R. E. and Slavin, J. A., Magnetic flux transfer associated with expansions and contractions of the dayside magnetosphere, *J. Geophys. Res.*, **83**, 3831, 1978,

and Holzer, R. E. and Slavin, J. A., A correlative study of magnetic flux transfer in the magnetosphere, *J. Geophys. Res.*, **84**, 2573, 1979.

Petrinec, S. P., Song, P., and Russell, C. T., Solar cycle variations in the size and shape of the magnetopause, *J. Geophys. Res.*, **96**, 7893–7896, 1991.

The shock foot thickness method for determining shock speeds is described in:

Gosling, J. T. and Thomsen, M. F., Specularly reflected ions, shock foot thickness, and shock velocity determination in space, *J. Geophys. Res.*, **90**, 9893, 1985.

The ensemble approach to θ_{Bnu} determination was introduced by:

Balogh, A., González-Esparza, J. A., Forsyth, R. J., Burton, M. E., Goldstein, B. E., Smith, E. J., and Bame, S. J., Interplanetary shock waves: Ulysses observations in and out of the ecliptic plane, *Space Sci. Rev.*, **72**, 171–180, 1995.